

pubs.acs.org/JPCL Letter

Inverted Lowest Singlet and Triplet Excitation Energy Ordering of Graphitic Carbon Nitride Flakes

Xiaopeng Wang,* Aizhu Wang, Mingwen Zhao, and Noa Marom



Cite This: J. Phys. Chem. Lett. 2023, 14, 10910-10919



Read Online

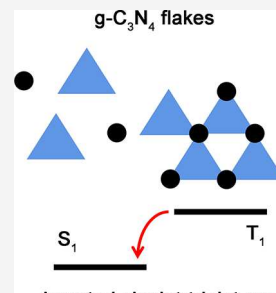
ACCESS I

III Metrics & More

Article Recommendations

SI Supporting Information

ABSTRACT: In organic light-emitting diodes (OLEDs), only 25% of electrically generated excitons are in a singlet state, S_1 , and the remaining 75% are in a triplet state, T_1 . In thermally activated delayed fluorescence (TADF) chromophores the transition from the nonradiative T_1 state to the radiative S_1 state can be thermally activated, which improves the efficiency of OLEDs. Chromophores with inverted energy ordering of S_1 and T_1 states, $S_1 < T_1$, are superior to TADF chromophores, thanks to the absence of an energy barrier for the transition from T_1 to S_1 . We benchmark the performance of time-dependent density functional theory using different exchange-correlation functionals and find that scaled long-range corrected double-hybrid functionals correctly predict the inverted singlet—triplet gaps of N-substituted phenalene derivatives. We then show that the inverted energy ordering of S_1 and T_1 is an intrinsic property of graphitic carbon nitride flakes. A design strategy of new chromophores with inverted singlet—triplet gaps is proposed. The color of emitted light can be fine-tuned through flake size and amine substitution on flake vertices.



inverted singlet-triplet gap

rganic light-emitting diodes (OLEDs) have attracted great interest for display and lighting applications. The efficiency of conventional OLEDs is low because 75% of electrically generated excitons are in a triplet state, whose radiative decay to the singlet ground state is forbidden by selection rules. Phosphorescent heavy-metal complexes were used in so-called second generation of OLEDs because heavy metal atoms enhance spin—orbit coupling and facilitate light emission from the triplet state. However, heavy metal atoms are environmentally hazardous. Thermally activated delayed fluorescence (TADF)^{4–9} chromophores used in third generation OLEDs are purely organic and may also possess a nearly 100% internal quantum efficiency, i.e., full conversion of all excitons into light.

In 2011, Endo et al. demonstrated that spatially separating the highest occupied molecular orbital (HOMO) and the lowest unoccupied molecular orbital (LUMO) leads to a very small electron exchange energy, resulting in a small energy gap, ΔE_{ST} , between the lowest singlet excited state, S_1 , and the lowest triplet excited state, T_1 . This enables thermal activation of the transition from the nonradiative T_1 state to the radiative S_1 state, followed by light emission from S_1 . They synthesized a donor—acceptor molecule whose HOMO and LUMO are separated and located on the donor and acceptor moieties, respectively. This chromophore was found to have a small ΔE_{ST} of 0.11 eV, leading to efficient TADF. In the past decade, numerous donor—acceptor TADF molecules have been experimentally synthesized and/or theoretically proposed. S_1 1,14

In 2015, Hatakeyama et al. proposed a new design strategy to separate the HOMO and LUMO, namely, multiple resonance (MR) induced TADF. 15,16 MR-TADF chromo-

phores are rigid polycyclic aromatic hydrocarbons (PAHs) doped with electron-donating atoms, such as N, simultaneously with electron-withdrawing atoms, such as B. The HOMO and LUMO are spatially separated on two groups of atoms due to the opposite resonance effect of electron-donating and electron-withdrawing atoms. Owing to their conformational rigidity, MR-TADF molecules have the advantage of a narrow emission peak and high color purity, compared to donor—acceptor TADF molecules. Additional MR-TADF chromophores have been experimentally synthesized and/or theoretically proposed. 17–31

The ΔE_{ST} of TADF molecules is positive, albeit small. According to Hund's multiplicity rule, in closed-shell organic molecules, the T_1 state should be lower in energy than the S_1 state. However, there exist a handful of compounds^{32–35} that violate Hund's rule. The inverted energy ordering of the S_1 and T_1 states leads to an energetically downhill reverse intersystem crossing (RISC) from T_1 to S_1 . Thanks to the absence of a thermal activation energy for RISC, such compounds are superior to TADF chromophores in OLED applications. Using a model system of cycl[3.3.3]-azine, shown in Figure 1a, de Silva theoretically demonstrated that a double excitation character of low-lying excited states is a prerequisite for the inversion of S_1 and T_1 .³²

Received: October 11, 2023 Revised: November 22, 2023 Accepted: November 28, 2023 Published: November 30, 2023





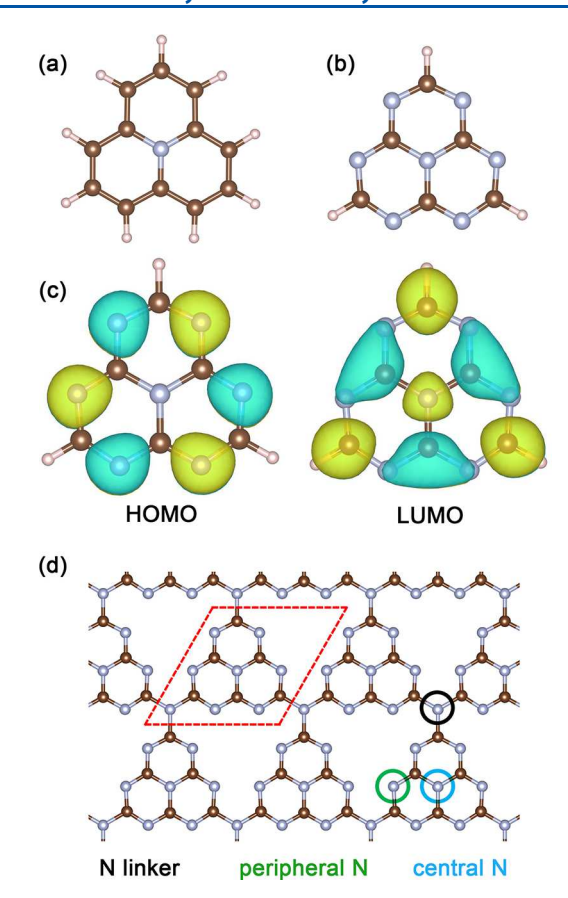


Figure 1. N-substituted phenalenes: (a) cycl[3.3.3]-azine and (b) heptazine. C, N, and H atoms are shown in brown, gray, and pink. (c) Frontier orbitals of heptazine visualized with an isosurface value of 0.03 au. (d) Heptazine-based graphitic carbon nitride.

Another N-substituted phenalene with a negative ΔE_{ST} is heptazine (Hz), shown in Figure 1b.³³ The singlet—triplet inversion has been attributed to the double excitation character of low-lying excited states and a small electron exchange energy due to minimized spatial overlap between the HOMO and LUMO.^{33,34} Similarly to the spatial separation of frontier orbitals of MR-TADF molecules, the HOMO of Hz is located

on the 6 peripheral electron-donating N atoms, whereas the LUMO is located on C atoms and the central N atom, as shown in Figure 1c. Pollice et al. computationally screened N-substituted and functionalized phenalenes and discovered some compounds exhibiting negative singlet—triplet gaps and substantial fluorescence rates, considered promising for OLEDs. In addition to molecules with an inherently negative ΔE_{ST} , it has been shown that the inversion may be facilitated by the stabilization of singlet states in exciplexes, i.e., complexes of two molecules where one is in an excited state, in a microcavity, or in polarizable environments.

Since 1989, various carbon nitride (C_3N_4) structures have been computationally proposed. ^{39–42} Graphitic carbon nitride (g-C₃N₄) structures, proposed in 1996, have been found to be the most stable. 43 In particular, the Hz-based g-C₃N₄, shown in Figure 1d, has been reported to be the most stable allotrope. 44-47 Hz-based $g-\hat{C}_3N_4$ is a two-dimensional material consisting of Hz and N linkers. Hz-based g-C₃N₄ has been extensively studied in the context of photocatalytic applications, such as degradation of pollutants, $^{48-54}$ water splitting, $^{55-60}$ and CO_2 reduction. $^{61-64}$ Here, we computationally explore the prospects of the C_3N_4 family of materials for new applications in high-efficiency OLEDs. First, we establish that time dependent density functional theory (TDDFT) based on spin scaled long-range corrected (LC) double hybrid functionals⁶⁵ correctly predicts the negative ΔE_{ST} of Hz. Second, using this method, we show that negative ΔE_{ST} is an intrinsic property of g-C₃N₄ flakes regardless of their size and shape. Third, we find that the S_1 energy, which corresponds to the color of the emitted light, can be fine-tuned by modifying the flake size and by amine substitution on flake vertices. Different building blocks and linking atoms/groups may be used to further improve the performance of g-C₃N₄ derivatives in OLEDs.

In order to assess prospective chromophores for use in OLEDs, it is desirable to have a computational method that is sufficiently efficient to screen a large number of candidates and that is sufficiently accurate to provide reliable predictions. Thanks to the appealing balance between accuracy and efficiency, TDDFT has been widely used for the prediction of excited state properties of molecules, 13,66,67 including

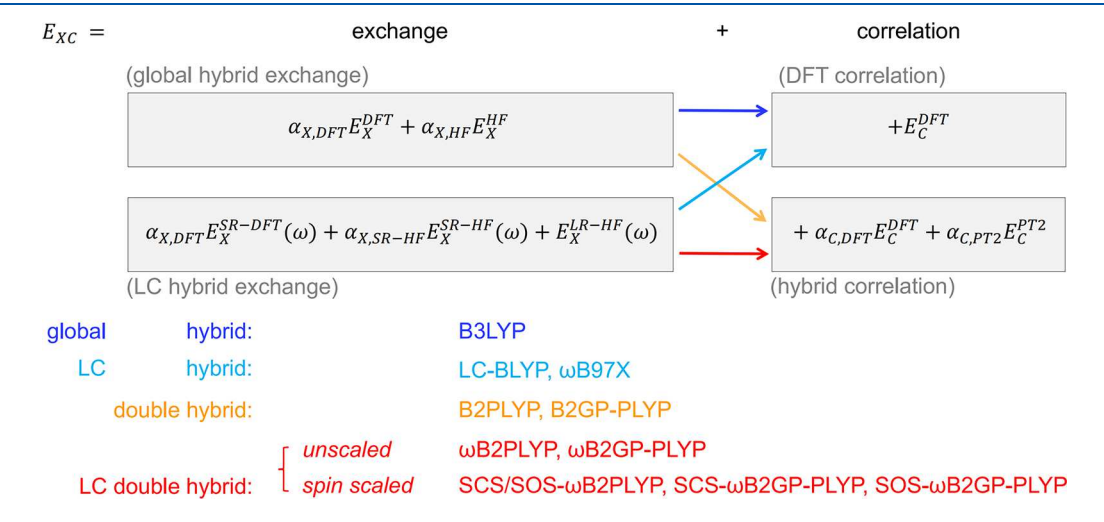


Figure 2. Schematic illustration of the combinations of exchange and correlation terms included in the global hybrid functionals (blue), LC hybrid functionals (cyan), double hybrid functionals (orange), and scaled and unscaled LC double hybrid functionals (red) benchmarked here for Hz. Fractions of different terms are denoted as α with a corresponding subscript.

chromophores with inverted singlet—triplet gaps.^{34,68–70} TDDFT is a formally exact theory, but its predictive power strongly depends on the choice of approximation to the exchange-correlation (xc) functional. Local and semilocal approximations may fail in the description of charge-transfer (CT) excited states, doubly excited states, and Rydberg states. Specifically, CT excitation energies may be significantly underestimated.^{14,71–78} The low-lying excited states of Hz are intramolecular CT states with substantial double excitation character. Therefore, we begin by benchmarking the performance of different classes of hybrid exchange-correlation functionals for Hz to determine which functionals are sufficiently reliable.

Figure 2 shows a schematic illustration of the combinations of exchange and correlation terms included in the B3LYP⁷⁶ global hybrid functional (blue), the LC-BLYP⁷⁷ and ω B97X⁷⁸ long-range corrected (LC) hybrid functionals (cyan), the B2PLYP⁷⁹ and B2GP-PLYP⁸⁰ double hybrid functionals (orange), the ω B2PLYP⁸¹ and ω B2GP-PLYP⁸¹ unscaled LC double hybrid functionals (red),⁸² and the spin-component scaled (SCS)⁸³ and spin-opposite scaled (SOS)^{83,84} LC double hybrid functionals (red).

In global hybrid functionals, a fraction of global exact exchange, $E_{\rm X}^{\rm HF}$, is mixed with the semilocal exchange, $E_{\rm X}^{\rm DFT}$, and correlation, $E_{\rm C}^{\rm DFT}$. This mitigates the effect of the selfinteraction error (SIE), 85-87 which causes underestimation of HOMO-LUMO gaps and destabilization of localized molecular orbitals. Correcting CT excitation energies requires a very large fraction of $E_{\rm X}^{\rm HF}$ in global hybrid functionals, which is detrimental to the overall accuracy. 86 To address this, LC hybrid functionals employ a range-splitting of the exact exchange term. These functionals contain a mixture of semilocal exchange and exact exchange in the short-range, $E_{\rm X}^{\rm SR-DFT}$ and $E_{\rm X}^{\rm SR-HF}$, and full exact exchange in the long-range, $E_{\rm x}^{\rm LR-HF}$. This ensures the correct $1/r_{12}$ decay of the potential, where $1/r_{12}$ is the interelectronic distance. The interplay between the short- and long-range is controlled by a rangeseparation parameter, ω . We previously benchmarked TDDFT for 16 donor-acceptor TADF chromophores and 3 MR-TADF chromophores. 14,31 Functionals with a full exact exchange in the long-range and a range separation parameter of about 0.30 bohr⁻¹ have been shown to provide a balanced description of valence excitations (between orbitals localized on the same region of the molecule) and intramolecular CT excitations. Considering the intramolecular CT character of the low-lying excited states of Hz, functionals with LC exchange are necessary for reliable treatment of Hz-based g-C₃N₄ flakes.

Some excited states may have a double excitation character, meaning a many-electron state that is dominated by a doubly excited Slater determinant with two electrons in occupied orbitals promoted to unoccupied orbitals. See Such states can be calculated with wave-function-based methods that include doubles. An alternative approach within the framework of TDDFT is to use double hybrid functionals, which include a perturbative second-order correlation, $E_{\rm C}^{\rm PT2}$, to account for doubly excited configurations, as shown in Figure 2. For example, the B2PLYP and B2GP-PLYP global double hybrid functionals and their range-separated variants, ω B2PLYP and ω B2GP-PLYP, apply a fraction, $\alpha_{\rm C,PT2}$, of Head-Gordon's configuration interaction singles with perturbative doubles $[{\rm CIS}({\rm D})]^{92}$ correction, $\Delta_{{\rm CIS}({\rm D})}$, to the TDDFT excitation energies obtained with global or LC hybrid functionals:

$$E_{\text{double-hybrid}}^{\text{TDDFT}} = E_{\text{hybrid}}^{\text{TDDFT}} + \alpha_{\text{C,PT2}} \Delta_{\text{CIS(D)}}$$
 (1)

It has been demonstrated in several studies that LC double hybrid functionals are useful for predicting the inverted singlet-triplet gaps of various chromophores. 34,68-70 We note, however, that TDDFT with global double hybrid functionals has been shown to yield a large deviation for double excitations in polyene molecules. ⁹⁴ The performance of TDDFT for transitions with double-excitation character may be improved by using scaled LC double hybrid functionals. The CIS(D) energy correction to the configuration interaction singles (CIS) total energy of an excited state has a "direct" term and an "indirect" term. These two terms can be broken down into same-spin and opposite-spin components with four scale parameters.⁹⁵ Readers are referred to refs 93 and 83 for the explicit form of the same- and opposite-spin terms and SCS and SOS settings of the four parameters. Using the appropriate SCS or SOS settings, $\Delta_{CIS(D)}$ in eq 1 is updated to produce TDDFT excitation energies with scaled LC double hybrid functionals. Casanova-Páez et al. benchmarked 8 unscaled and 14 scaled global and LC double hybrid functionals for 203 excitations of different molecules and different excitation types.⁸³ The benefit of using SCS and SOS is a more accurate description, with mean deviations typically being closer to zero. Unlike some ground-state wave function methods where SOS leads to inferior results compared to SCS, 96,97 the SCS and SOS variants of double-hybrid functionals show negligible differences of 0.03 eV at most in the root-mean-square deviations of excitation energies.85

To assess the reliability of TDDFT for the compounds studied here, we benchmark global, unscaled, and scaled LC double hybrid functionals specifically for the building block of $g\text{-}C_3N_4$, Hz. The $S_1 \to S_0$ transition of Hz is dipole-forbidden, and no experimental data are available for T_1 . Therefore, the results of high-level quantum chemistry methods are used as reference values. Several multireference methods have been employed to study excited states of Hz and similar molecules in different groups. $^{33,70,98-102}$ Table 1 shows the excitation energies of Hz, obtained using TDDFT with different exchange-correlation functionals, compared to example reference values 33 obtained using second-order algebraic diagrammatic construction [ADC(2)], 103 third-order algebraic diagrammatic construction [ADC(3)], approximate coupled cluster singles-and-doubles (CC2), 104 equation-of-motion singles-and-doubles coupled cluster (EOM-CCSD), 105 and multiconfigurational second-order perturbation theory (CASPT2).

The S_1 excitation energies produced by ADC(2), ADC(3), CC2, EOM-CCSD, and CASPT2 range from 2.326 eV (533 nm) to 2.81 eV (441 nm), corresponding to green to violet light. The S_1 excitation energies produced by TDDFT are higher, on average, ranging from 2.779 to 3.137 eV. The T_1 reference values range from 2.551 to 2.963 eV. The TDDFT T_1 values are also higher on average, ranging from 2.716 to 3.104 eV. Overall, global hybrid functionals and global double hybrid functionals slightly overestimate the S_1 excitation energy, whereas the T_1 excitation energies are close to those of ADC(2), ADC(3), CC2, EOM-CCSD, and CASPT2. The S_1 and T_1 excitation energies obtained with LC hybrid functionals and unscaled LC double hybrid functionals further increase owing to the larger fraction of exact exchange in the long-range. The overestimations of ω B2PLYP and ω B2GP-PLYP are partly corrected by their SCS and SOS variants, but

Table 1. Excitation Energies of Hz Obtained with ADC(2), CC2, EOM-CCSD, CASPT2, and TDDFT Using Different Exchange-Correlation Functionals^a

Methods	S_1	T_1	ΔE_{ST}
$ADC(2)^{b}$	2.569	2.851	-0.282
$ADC(2)^c$	2.68	2.92	-0.24
$ADC(3)^c$	2.81	2.88	-0.07
$CC2^{b}$	2.676	2.947	-0.271
EOM-CCSD ^b	2.781	2.963	-0.182
CASPT2 ^b	2.326	2.551	-0.225
B3LYP	2.936	2.716	0.220
LC-BLYP	3.118	2.848	0.270
ω B97X	3.292	3.016	0.276
B2PLYP	2.782	2.813	-0.031
B2GP-PLYP	2.845	2.928	-0.083
ω B2PLYP	3.137	3.067	0.070
ω B2GP-PLYP	3.100	3.104	-0.004
$SCS/SOS-\omega B2PLYP^d$	2.918	3.029	-0.111
SCS- ω B2GP-PLYP	2.779	2.963	-0.184
SOS- ω B2GP-PLYP	2.805	3.041	-0.236

^aAll values are in eV. ^bReference values are from ref 33. ^cReference values are from ref 98. ^dSCS- ω B2PLYP and SOS- ω B2PLYP functionals have the same parameters. ⁸³

the excitation energies are still higher than reference values. The TDDFT excitation energies obtained with the B2PLYP, ω B2PLYP, and SCS/SOS- ω B2PLYP functionals agree well with the values reported in ref 68 with differences of less than 0.01 eV in ΔE_{ST} .

All of the reference methods correctly predict an inverted singlet—triplet gap. The ΔE_{ST} values of ADC(2) and CC2 are very close and smaller than those of others. The ADC(3) ΔE_{ST} is the largest but still negative. In contrast, TDDFT does not consistently predict an inverted singlet—triplet gap. The B3LYP global hybrid functional and the LC-BLYP and ω B97X LC hybrid functionals incorrectly yield a positive

 ΔE_{ST} . We attribute this to the lack of a perturbative correlation component to account for doubly excited configurations. With the B2PLYP and B2GP-PLYP double hybrid functionals, ΔE_{ST} turns slightly negative, close to the reference value of ADC(3). The use of range separated exchange to balance the description of valence excitations and intramolecular CT excitations in the ω B2PLYP and ω B2GP-PLYP LC double hybrid functionals does not significantly change the ΔE_{ST} compared to B2PLYP and B2GP-PLYP. However, with TDDFT@ ω B2PLYP ΔE_{ST} becomes slightly positive. This small change is determined by the similar CT character of the S_1 and T_1 excited states of Hz. Specifically, the transition from HOMO to LUMO contributes 94% and 92% to the TDDFT@ ω B2PLYP S_1 and T_1 states.

With the scaled LC double hybrid functionals SCS/SOSωB2PLYP, SCS-ωB2GP-PLYP, and SOS-ωB2GP-PLYP, TDDFT yields negative ΔE_{ST} values that are quantitatively closer to the reference values. For example, TDDFT@SCS- ω B2GP-PLYP produces S_1 , T_1 , and ΔE_{ST} values that are within 0.002 eV of the EOM-CCSD values. This indicates that TDDFT with scaled LC double hybrid functionals, where LC exchange and scaled perturbative correlation are added to DFT exchange and correlation, is an efficient and accurate approach for calculating excited states exhibiting CT and double excitation character, such as those of chromophores with negative ΔE_{ST} . To show that this conclusion can be generalized, we have compiled a benchmark set of 10 Nsubstituted phenalene derivatives, shown in Figure S1 in the Supporting Information. For these compounds, experimental values are available for the S_1 excitation energies $^{107-112}$ and EOM-CCSD and ADC(2) values are available for S_1 and T_1 . Tables S1-S3 and Figure S2 show that the trends observed here for Hz persist across the entire benchmark set. TDDFT with LC double hybrid functionals correctly reproduce the qualitative trends in the relative energies of S_1 and T_1 among different molecules. However, with the unscaled LC double hybrid functionals, TDDFT overestimates the S_1 excitation energies by about 0.3 eV, leading to larger (more positive)

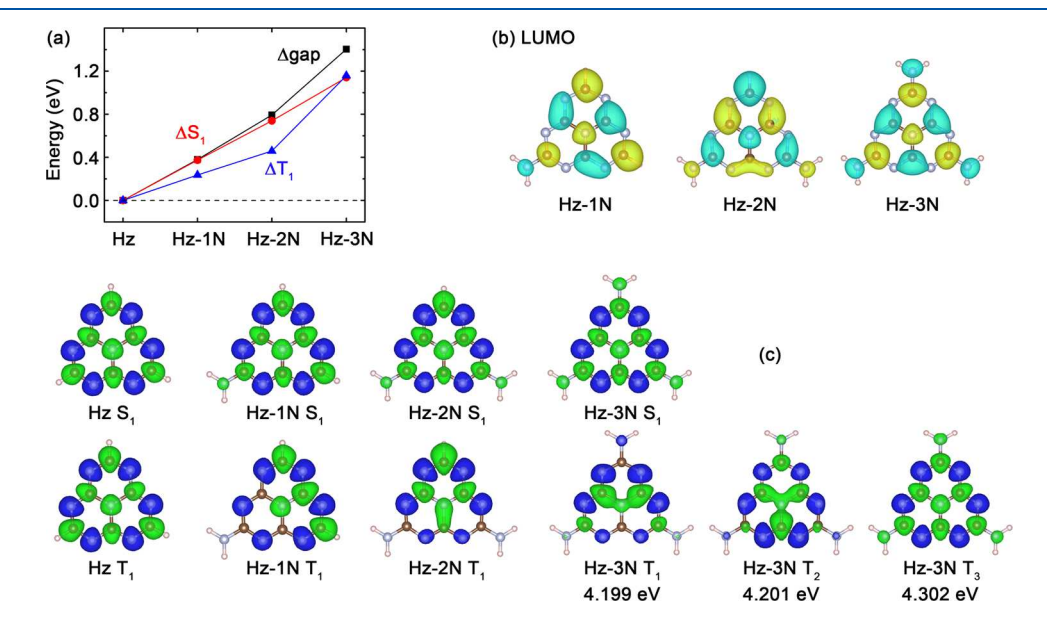


Figure 3. (a) TDDFT@SOS- ω B2GP-PLYP HOMO–LUMO gap, S_1 , and T_1 energies of amine-substituted Hz referenced to Hz. (b) LUMO of amine-substituted Hz visualized with an isosurface value of 0.03 au. (c) Electron density difference, $\Delta \rho$, between low-lying excited states and ground states visualized with an isosurface value of 0.002 au. The green and blue represent positive $\Delta \rho$ (electron gain) and negative $\Delta \rho$ (electron loss).

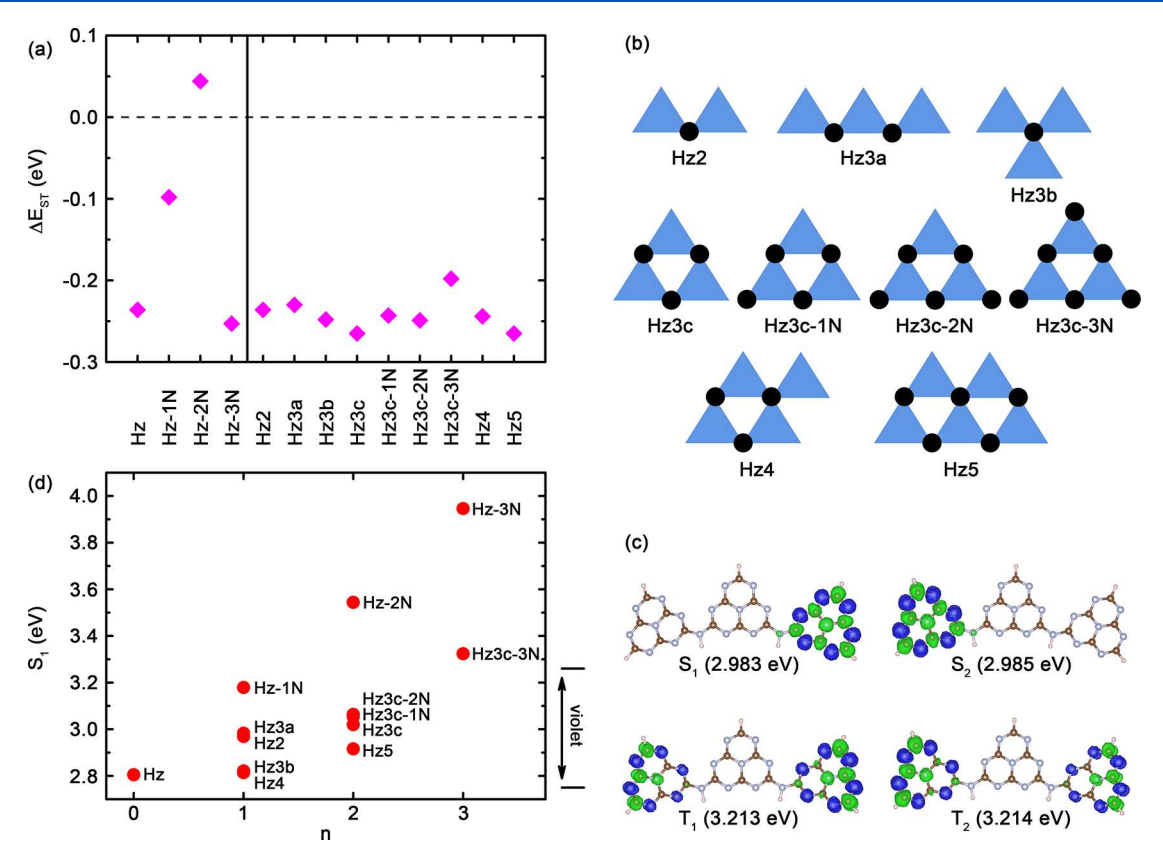


Figure 4. (a) TDDFT@SOS- ω B2GP-PLYP ΔE_{ST} of Hz, Hz-xN, and g-C₃N₄ flakes. (b) Hz-based g-C₃N₄ flakes and their labels. The blue triangles represent the Hz moieties, and the black circles represent N linkers or amine side-groups on vertices. (c) Electron density difference, $\Delta \rho$, between low-lying excited states and the ground state of the Hz3a flake, obtained with TDDFT@SOS- ω B2GP-PLYP, visualized with an isosurface value of 0.002 au. The green and blue represent positive $\Delta \rho$ (electron gain) and negative $\Delta \rho$ (electron loss). (d) TDDFT@SOS- ω B2GP-PLYP S_1 energies of Hz, Hz-xN, and g-C₃N₄ flakes. n is the lowest number of N linkers or amine groups bonded to any of the Hz moieties in a g-C₃N₄ flake.

 ΔE_{ST} values than those of EOM-CCSD and ADC(2). With the scaled LC double hybrid functionals, the TDDFT S_1 and T_1 excitation energies agree quantitatively with the reference values. In particular, TDDFT@SOS- ω B2GP-PLYP ΔE_{ST} energies exhibit the same sign as those obtained with EOM-CCSD across the benchmark set, i.e., eight negative and two positive ΔE_{ST} values. Based on this, we henceforth use TDDFT with scaled LC double hybrid functionals to study the singlet—triplet gaps of graphitic carbon nitride derivatives.

For the OLEDs, it is desirable to tune the S_1 energy to achieve a range of colors. We then examined whether the S_1 energy of Hz can be tuned by side-group substitutions. Because Hz moieties in g-C₃N₄ are linked by N atoms, we study the properties of amine-substituted Hz molecules, Hz-xN, where x = 1–3 indicates the number of H atoms substituted by amine groups. Hz-3N, i.e., melem, is an efficient luminescent material. The HOMO–LUMO gaps of Hz-xN increase with the number of amine groups, as shown in Figure 3a.

In addition to orbital energies, amine substitution affects the spatial distribution of frontier orbitals. The HOMOs of Hz-xN are located on the 6 peripheral N atoms of Hz, similar to the HOMO of Hz. The LUMOs are extended to the amine groups of Hz-xN, as shown in Figure 3b. This is consistent with our previous observation that in other MR-TADF chromophores the HOMO (or LUMO) is extended to substituents attached to electron donating (or withdrawing) atoms. For Hz-1N and Hz-2N, the LUMO distribution on the Hz skeleton is slightly shifted toward the peripheral N atoms farther from the

amine substituents, increasing the overlap between the HOMO and LUMO.

The effect of amine substitution on the energies and spatial distribution of the molecular orbital propagates to excited-state properties. As shown in Figure 3a, the changes in the S_1 and T_1 excitation energies track the change in the HOMO-LUMO gap. This is because these excited states are dominated by the transition from HOMO to LUMO, except for the T_1 excitation of Hz-3N (the spectral decomposition of these states is provided in the Supporting Information). Electron density differences between low-lying excited states and ground states, $\Delta \rho$, are visualized for Hz and Hz-xN in Figure 3c. In general, the electron charge is transferred from the six peripheral N atoms to the C atoms and the central N atom, similar to the case for unsubstituted Hz. For the S_1 states of Hz-xN, there is also electron gain on the amine groups because of the extended LUMO distribution. For the T_1 states of Hz-1N and Hz-2N, the electron gain on the amine group vanishes. For Hz-3N, the three lowest triplet excited states, T_1 , T_2 , and T_3 , are very close in energy. T₃ is dominated by the transition from HOMO to LUMO and has a similar $\Delta \rho$ distribution to the singlet state, S_1 (the spectral decomposition of T_1 , T_2 , and T_3 is provided in the Supporting Information).

Amine substitution also affects ΔE_{ST} , which increases from Hz to Hz-1N, and further increases to a small positive value for Hz-2N, as shown in Figure 4a. A negative ΔE_{ST} stems from both double excitation character of low-lying excited states, as demonstrated by de Silva,³² and minimal spatial overlap between the HOMO and LUMO. The increase of ΔE_{ST} for

Hz-1N and Hz-2N may be attributed to increased overlap between the HOMO and LUMO. ΔE_{ST} of Hz-3N is close to that of Hz, which may be attributed to the similar HOMO and LUMO distributions. Hz- α N molecules are suitable for OLEDs in terms of ΔE_{ST} . Hz-1N and Hz-3N still exhibit an energetically downhill RISC. Hz-2N is an MR-TADF chromophore with a very small energy barrier to RISC. In terms of the excitation energy, substitution with one amine group shifts the emitted light to the high-energy end of the visible spectrum. A larger number of amine groups, as in Hz-3N, increases S_1 beyond the visible range.

The effect of amine substitution on the excitation energies of Hz derivatives is also manifested in the excited-state properties of Hz-based g- C_3N_4 flakes. We consider a set of nine g- C_3N_4 flakes of different sizes and shapes, with a varying number of amine groups attached to their vertices, as shown in Figure 4b.

Different Hz moieties in the same flake may be linked to different numbers of N linkers. For example, in the Hz3a flake, the two peripheral Hz moieties are linked to one N atom, whereas the middle Hz moiety is linked to two N atoms. Based on the excitation energy analysis of Hz-xN above, we expect the excitons located on the peripheral Hz moieties of Hz3a to have a lower energy than the exciton localized on the middle Hz moiety. This is confirmed by the electron density difference between the low-lying excited states and the ground state, shown in Figure 4c. The molecule's symmetry leads to degeneracy in the energies of S_1 and S_2 and T_1 and T_2 . All four low-lying excited states are located on the peripheral Hz moieties of Hz3a, which have fewer N linkers than the middle Hz moiety. This trend in spatial localization of low-lying excited states is also observed in other g-C₃N₄ flakes, as shown in the Supporting Information. For g-C₃N₄ flakes with amine side groups, the low-lying excited states tend to be localized on Hz moieties with unsubstituted vertices independent of the overall flake size and shape.

We define a parameter, *n*, as the lowest number of N linkers or amine groups bonded to any of the Hz moieties in a g-C₃N₄ flake, which is 1 in the case of Hz3a. The parameter n affects the spatial distribution and energies of the low-lying excited states of the g-C₃N₄ flakes. Figure 4d shows the TDDFT@ SOS- ω B2GP-PLYP S_1 energies of Hz, Hz-xN, and g-C₃N₄ flakes (values obtained with other scaled LC double hybrid functionals are provided in the Supporting Information). The S_1 energy increases with the number of amine substitutions, i.e., with n, in Hz, Hz-1N, Hz-2N, and Hz-3N, as shown in Figures 3a and 4d. Another example is Hz3c, Hz3c-1N, Hz3c-2N, and Hz3c-3N, which have the same flake shape but different numbers of amine substitutions. The former three flakes have the same n of 2 and consequently very close S_1 energies around 3.040 eV. In comparison, the latter flake, Hz3c-3N, has a larger n of 3, and thus a larger S_1 energy of 3.324 eV. In addition to n, the S_1 energy depends on the flake size. Within a family of flakes with the same n, the S_1 energy generally decreases as the flake size increases, which may be attributed to the quantum size effect.

This leads to a two-parameter approach to fine-tune the color of emitted light by modifying the flake size and amine substitutions on flake vertices. For the flakes considered here, the S_1 energy varies over a range of about 0.5 eV above that of the parent Hz compound, which corresponds to a decrease in wavelength of about 70 nm. This would correspond to tuning from, e.g., green to blue or blue to purple. We note, however, that because of the uncertainty in our calculations, with the

reference values for the S_1 energy of Hz ranging from 2.326 to 2.81 eV (green to violet region), we cannot reliably predict the exact emission color of the chromophores studied here. Different linking atoms or side-groups may be used to shift the color of emitted light toward the lower-energy end of the visible range, further extending the color range of Hz-based chromophores. For example, using electron-withdrawing groups instead of amine substituents on Hz has been found to decrease the S_1 energy while preserving the negative ΔE_{ST} . The state of the state o

Figure 4a shows the ΔE_{ST} of Hz, Hz-xN, and g-C₃N₄ flakes obtained with TDDFT@SOS- ω B2GP-PLYP. Tabulated TDDFT excitation energies and ΔE_{ST} of g-C₃N₄ flakes obtained with SCS/SOS- ω B2PLYP, SCS- ω B2GP-PLYP, and SOS- ω B2GP-PLYP functionals are provided in the Supporting Information. Apart from the higher values for Hz-1N and Hz-2N, ΔE_{ST} is between -0.3 and -0.2 eV, corresponding to a downhill RISC process, which is favorable for OLEDs. Based on the set of g-C₃N₄ flakes of different sizes and shapes, and a varying number of amine side-groups on vertices, we infer that the inverted lowest singlet and triplet excitation energy ordering is an intrinsic and robust property of g-C₃N₄ flakes, echoing reports of Hz derivative single molecules and Hz polymers. ^{32,33,116}

In summary, in search of candidate materials for highperformance OLEDs, we have investigated a family of graphitic carbon nitride flakes, composed of Hz building blocks, which possess an inverted energy ordering of S_1 and T_1 . The negative ΔE_{ST} has been attributed to a combination of minimal spatial overlap between frontier orbitals and the double excitation character of low-lying excited states. Based on a benchmark set of 10 N-substituted phenalene derivatives, we have shown that TDDFT with scaled LC double hybrid functionals correctly predicts inverted singlet-triplet gaps and produces ΔE_{ST} values in quantitative agreement with reference values of high-level quantum chemistry methods. We attribute the success of scaled LC double hybrid functionals to the inclusion of full exact exchange in the long-range and scaled perturbative correlation. The exact exchange term mitigates the effect of the SIE and ensures the correct $1/r_{12}$ decay of the potential, improving the description of CT excitations. The scaled perturbative correlation term is necessary for the correct treatment of double excitations. Therefore, we recommend TDDFT with scaled LC double hybrid functionals for a reliable assessment of prospective chromophores with a negative ΔE_{ST} .

The inverted energy ordering of S_1 and T_1 has been reported for single molecules of Hz derivatives and polymeric Hz. 32,33,100,116 We have demonstrated that the inverted singlet-triplet gap is also an inherent property of Hz-based g-C₃N₄ flakes, which persists independent of the flake size and shape. Furthermore, the S_1 energy, corresponding to the color of the emitted light, can be fine-tuned via a two-pronged approach of altering the flake size and functionalizing the flake vertices. Based on this, we may propose a strategy for computationally designing chromophores with high fluorescence rates, downhill RISC, and tunable colors for use in highefficiency OLEDs. The starting point is choosing compounds out of the family of N-substituted and functionalized phenalenes, which possess a negative ΔE_{ST} and exhibit high fluorescence rates.³⁴ These compounds can then be used as building blocks for graphitic carbon nitride flakes while preserving their inverted singlet-triplet gaps. Finally, the S_1 energies, corresponding to the color of emitted light, can be

fine-tuned by changing the flake size and by chemical substitutions at the flake vertices, as exemplified in the case of $g-C_3N_4$. This design strategy opens up exciting prospects for high-performance, layered-based OLEDs based on carbon nitride derivatives.

COMPUTATIONAL DETAILS

All calculations were performed with version 5.0.0 of the ORCA code. 117,118 Molecular geometries were optimized with the def2-TZVP basis sets 119 and the ω B97X-D3 functional, 120 which incorporates the empirical atom—atom dispersion corrections from DFT-D3. 121 Tight SCF convergence criteria corresponding to an energy tolerance of 1 \times 10 $^{-8}$ au were applied. DefGrid2 grids were used. 122 The Def2-TZVP and def2-TZVP/C auxiliary basis set 123 were utilized in the TDDFT calculations with double hybrid and LC double hybrid functionals. We previously demonstrated the convergence of this basis set in TDDFT calculations. 14 The Tamm—Dancoff approximation was not used.

ASSOCIATED CONTENT

Data Availability Statement

The authors confirm that the data supporting the findings of this study are available within the article and its Supporting Information.

Solution Supporting Information

The Supporting Information is available free of charge at https://pubs.acs.org/doi/10.1021/acs.jpclett.3c02835.

Benchmark of TDDFT, spectral composition, frontier orbitals, electron density difference, and excitation energies of carbon nitride flakes (PDF)

AUTHOR INFORMATION

Corresponding Author

Xiaopeng Wang — School of Foundational Education, University of Health and Rehabilitation Sciences, Qingdao 266114, China; Qingdao Institute for Theoretical and Computational Sciences, Institute of Frontier and Interdisciplinary Science, Shandong University, Qingdao, Shandong 266237, P. R. China; orcid.org/0000-0001-6866-4864; Email: wangxiaopeng@uor.edu.cn

Authors

Aizhu Wang — Collaborative Innovation Center of Technology and Equipment for Biological Diagnosis and Therapy in Universities of Shandong, Institute for Advanced Interdisciplinary Research (iAIR), University of Jinan, Jinan 250022, P. R. China; orcid.org/0000-0003-2297-5426

Mingwen Zhao — School of Physics and State Key Laboratory of Crystal Materials, Shandong University, Jinan, Shandong 250100, China; orcid.org/0000-0002-7583-9682

Noa Marom — Department of Materials Science and Engineering, Carnegie Mellon University, Pittsburgh, Pennsylvania 15213, United States; Department of Physics and Department of Chemistry, Carnegie Mellon University, Pittsburgh, Pennsylvania 15213, United States; orcid.org/0000-0002-1508-1312

Complete contact information is available at: https://pubs.acs.org/10.1021/acs.jpclett.3c02835

Notes

The authors declare no competing financial interest.

ACKNOWLEDGMENTS

The authors thank the Natural Science Foundation of Shandong Province, China (Grant No. ZR2020QB073). Work at CMU was supported by the National Science Foundation (NSF) Division of Materials Research through grant DMR-2021803. This research used resources of the Shandong QuickCalc Technology Co., Ltd and the Shandong Bailing Cloud Computing Co., Ltd.

REFERENCES

- (1) Hong, G.; Gan, X.; Leonhardt, C.; Zhang, Z.; Seibert, J.; Busch, J. M.; Bräse, S. A Brief History of OLEDs Emitter Development and Industry Milestones. *Adv. Mater.* **2021**, *33*, 2005630.
- (2) Reineke, S.; Thomschke, M.; Lüssem, B.; Leo, K. White Organic Light-Emitting Diodes: Status and Perspective. *Rev. Mod. Phys.* **2013**, 85, 1245.
- (3) Geffroy, B.; Le Roy, P.; Prat, C. Organic Light-Emitting Diode (OLED) Technology: Materials, Devices and Display Technologies. *Polym. Int.* **2006**, *55*, 572–582.
- (4) Parker, C. A.; Hatchard, C. G. Triplet-Singlet Emission in Fluid Solutions. Phosphorescence of Eosin. *Trans. Faraday Soc.* **1961**, *57*, 1894–1904.
- (5) Yang, Z.; Mao, Z.; Xie, Z.; Zhang, Y.; Liu, S.; Zhao, J.; Xu, J.; Chi, Z.; Aldred, M. P. Recent Advances in Organic Thermally Activated Delayed Fluorescence Materials. *Chem. Soc. Rev.* **2017**, *46*, 915–1016.
- (6) Tao, Y.; Yuan, K.; Chen, T.; Xu, P.; Li, H.; Chen, R.; Zheng, C.; Zhang, L.; Huang, W. Thermally Activated Delayed Fluorescence Materials towards the Breakthrough of Organoelectronics. *Adv. Mater.* **2014**, *26*, 7931–7958.
- (7) Wong, M. Y.; Zysman-Colman, E. Purely Organic Thermally Activated Delayed Fluorescence Materials for Organic Light-Emitting Diodes. *Adv. Mater.* **2017**, *29*, 1605444.
- (8) Liu, Y.; Li, C.; Ren, Z.; Yan, S.; Bryce, M. R. All-Organic Thermally Activated Delayed Fluorescence Materials for Organic Light-Emitting Diodes. *Nat. Rev. Mater.* **2018**, *3*, 1–20.
- (9) Bryden, M. A.; Zysman-Colman, E. Organic Thermally Activated Delayed Fluorescence (TADF) Compounds Used in Photocatalysis. *Chem. Soc. Rev.* **2021**, *50*, 7587–7680.
- (10) Sun, J. W.; Lee, J.-H.; Moon, C.-K.; Kim, K.-H.; Shin, H.; Kim, J.-J. A Fluorescent Organic Light-Emitting Diode with 30% External Quantum Efficiency. *Adv. Mater.* **2014**, *26*, 5684–5688.
- (11) Kaji, H.; Suzuki, H.; Fukushima, T.; Shizu, K.; Suzuki, K.; Kubo, S.; Komino, T.; Oiwa, H.; Suzuki, F.; Wakamiya, A.; et al. Purely Organic Electroluminescent Material Realizing 100% Conversion from Electricity to Light. *Nat. Commun.* **2015**, *6*, 8476.
- (12) Endo, A.; Sato, K.; Yoshimura, K.; Kai, T.; Kawada, A.; Miyazaki, H.; Adachi, C. Efficient Up-Conversion of Triplet Excitons into a Singlet State and its Application for Organic Light Emitting Diodes. *Appl. Phys. Lett.* **2011**, *98*, 083302.
- (13) Gómez-Bombarelli, R.; Aguilera-Iparraguirre, J.; Hirzel, T. D.; Duvenaud, D.; Maclaurin, D.; Blood-Forsythe, M. A.; Chae, H. S.; Einzinger, M.; Ha, D.-G.; Wu, T.; et al. Design of Efficient Molecular Organic Light-Emitting Diodes by a High-Throughput Virtual Screening and Experimental Approach. *Nat. Mater.* **2016**, *15*, 1120–1127.
- (14) Wang, X.; Gao, S.; Zhao, M.; Marom, N. Benchmarking Time-Dependent Density Functional Theory for Singlet Excited States of Thermally Activated Delayed Fluorescence Chromophores. *Phys. Rev. Res.* **2022**, *4*, 033147.
- (15) Hirai, H.; Nakajima, K.; Nakatsuka, S.; Shiren, K.; Ni, J.; Nomura, S.; Ikuta, T.; Hatakeyama, T. One-Step Borylation of 1,3-Diaryloxybenzenes Towards Efficient Materials for Organic Light-Emitting Diodes. *Angew. Chem., Int. Ed.* **2015**, *54*, 13581–13585.
- (16) Hatakeyama, T.; Shiren, K.; Nakajima, K.; Nomura, S.; Nakatsuka, S.; Kinoshita, K.; Ni, J.; Ono, Y.; Ikuta, T. Ultrapure Blue Thermally Activated Delayed Fluorescence Molecules: Efficient

- HOMO-LUMO Separation by the Multiple Resonance Effect. *Adv. Mater.* **2016**, 28, 2777–2781.
- (17) Hall, D.; Suresh, S. M.; dos Santos, P. L.; Duda, E.; Bagnich, S.; Pershin, A.; Rajamalli, P.; Cordes, D. B.; Slawin, A. M.; Beljonne, D.; et al. Improving Processability and Efficiency of Resonant TADF Emitters: A Design Strategy. *Adv. Opt. Mater.* **2020**, *8*, 1901627.
- (18) Jiang, P.; Miao, J.; Cao, X.; Xia, H.; Pan, K.; Hua, T.; Lv, X.; Huang, Z.; Zou, Y.; Yang, C. Quenching-Resistant Multiresonance TADF Emitter Realizes 40% External Quantum Efficiency in Narrowband Electroluminescence at High Doping Level. *Adv. Mater.* 2022, 34, 2106954.
- (19) Matsui, K.; Oda, S.; Yoshiura, K.; Nakajima, K.; Yasuda, N.; Hatakeyama, T. One-Shot Multiple Borylation Toward BN-Doped Nanographenes. *J. Am. Chem. Soc.* **2018**, *140*, 1195–1198.
- (20) Liang, X.; Yan, Z.-P.; Han, H.-B.; Wu, Z.-G.; Zheng, Y.-X.; Meng, H.; Zuo, J.-L.; Huang, W. Peripheral Amplification of Multi-Resonance Induced Thermally Activated Delayed Fluorescence for Highly Efficient OLEDs. *Angew. Chem., Int. Ed.* **2018**, *130*, 11486–11490.
- (21) Han, S. H.; Jeong, J. H.; Yoo, J. W.; Lee, J. Y. Ideal Blue Thermally Activated Delayed Fluorescence Emission Assisted by a Thermally Activated Delayed Fluorescence Assistant Dopant Through a Fast Reverse Intersystem Crossing Mediated Cascade Energy Transfer Process. J. Mater. Chem. C 2019, 7, 3082–3089.
- (22) Kondo, Y.; Yoshiura, K.; Kitera, S.; Nishi, H.; Oda, S.; Gotoh, H.; Sasada, Y.; Yanai, M.; Hatakeyama, T. Narrowband Deep-Blue Organic Light-Emitting Diode Featuring an Organoboron-Based Emitter. *Nat. Photonics* **2019**, *13*, 678–682.
- (23) Yuan, Y.; Tang, X.; Du, X.-Y.; Hu, Y.; Yu, Y.-J.; Jiang, Z.-Q.; Liao, L.-S.; Lee, S.-T. The Design of Fused Amine/Carbonyl System for Efficient Thermally Activated Delayed Fluorescence: Novel Multiple Resonance Core and Electron Acceptor. *Adv. Opt. Mater.* 2019, 7, 1801536.
- (24) Li, X.; Shi, Y.-Z.; Wang, K.; Zhang, M.; Zheng, C.-J.; Sun, D.-M.; Dai, G.-L.; Fan, X.-C.; Wang, D.-Q.; Liu, W.; et al. Thermally Activated Delayed Fluorescence Carbonyl Derivatives for Organic Light-Emitting Diodes with Extremely Narrow Full Width at Half-Maximum. ACS Appl. Mater. Interfaces 2019, 11, 13472–13480.
- (25) Wu, X.; Su, B.-K.; Chen, D.-G.; Liu, D.; Wu, C.-C.; Huang, Z.-X.; Lin, T.-C.; Wu, C.-H.; Zhu, M.; Li, E. Y.; et al. The Role of Host—Guest Interactions in Organic Emitters Employing MR-TADF. *Nat. Photonics* **2021**, *15*, 780–786.
- (26) Gao, H.; Shen, S.; Qin, Y.; Liu, G.; Gao, T.; Dong, X.; Pang, Z.; Xie, X.; Wang, P.; Wang, Y. Ultrapure Blue Thermally Activated Delayed Fluorescence (TADF) Emitters Based on Rigid Sulfur/Oxygen-Bridged Triarylboron Acceptor: MR TADF and D—A TADF. *J. Phys. Chem. Lett.* **2022**, *13*, 7561–7567.
- (27) Madayanad Suresh, S.; Hall, D.; Beljonne, D.; Olivier, Y.; Zysman-Colman, E. Multiresonant Thermally Activated Delayed Fluorescence Emitters Based on Heteroatom-Doped Nanographenes: Recent Advances and Prospects for Organic Light-Emitting Diodes. *Adv. Funct. Mater.* **2020**, *30*, 1908677.
- (28) Lin, S.; Ou, Q.; Shuai, Z. Computational Selection of Thermally Activated Delayed Fluorescence (TADF) Molecules with Promising Electrically Pumped Lasing Property. *ACS Mater. Lett.* **2022**, *4*, 487–496.
- (29) Di, K.; Guo, R.; Wang, Y.; Lv, Y.; Su, H.; Zhang, Q.; Yang, B.; Wang, L. Achieving High-Performance Narrowband Blue MR-TADF Emitter by Suppressing Isomer Formation and Extending π -Conjugate Skeleton. *J. Mater. Chem. C* **2023**, *11*, 6429.
- (30) Yang, W.; Miao, J.; Hu, F.; Zou, Y.; Zhong, C.; Gong, S.; Yang, C. An Effective Approach toward Yellow-to-Orange Multi-Resonance TADF Emitters by Integrating Strong Electron Donor into B/N-Based Polycyclic Architecture: High Performance OLEDs with Nearly 40% EQE. Adv. Funct. Mater. 2023, 33, 2213056.
- (31) Wang, X.; Gao, S.; Wang, A.; Wang, B.; Marom, N. Multiple Resonance Induced Thermally Activated Delayed Fluorescence: Effect of Chemical Modification. *Electron. Struct.* **2023**, *5*, 014010.

- (32) de Silva, P. Inverted Singlet—Triplet Gaps and Their Relevance to Thermally Activated Delayed Fluorescence. *J. Phys. Chem. Lett.* **2019**, *10*, 5674–5679.
- (33) Ehrmaier, J.; Rabe, E. J.; Pristash, S. R.; Corp, K. L.; Schlenker, C. W.; Sobolewski, A. L.; Domcke, W. Singlet—Triplet Inversion in Heptazine and in Polymeric Carbon Nitrides. *J. Phys. Chem. A* **2019**, 123, 8099–8108.
- (34) Pollice, R.; Friederich, P.; Lavigne, C.; dos Passos Gomes, G.; Aspuru-Guzik, A. Organic Molecules with Inverted Gaps between First Excited Singlet and Triplet States and Appreciable Fluorescence Rates. *Matter* **2021**, *4*, 1654–1682.
- (35) Kollmar, H.; Staemmler, V. Violation of Hund's Rule by Spin Polarization in Molecules. *Theor. Chim. Acta* **1978**, *48*, 223–239.
- (36) Difley, S.; Beljonne, D.; Van Voorhis, T. On the Singlet-Triplet Splitting of Geminate Electron-Hole Pairs in Organic Semiconductors. *J. Am. Chem. Soc.* **2008**, *130*, 3420–3427.
- (37) Eizner, E.; Martínez-Martínez, L. A.; Yuen-Zhou, J.; Kéna-Cohen, S. Inverting Singlet and Triplet Excited States Using Strong Light-Matter Coupling. *Sci. Adv.* **2019**, *5*, No. eaax4482.
- (38) Olivier, Y.; Yurash, B.; Muccioli, L.; D'Avino, G.; Mikhnenko, O.; Sancho-Garcia, J.-C.; Adachi, C.; Nguyen, T.-Q.; Beljonne, D. Nature of the Singlet and Triplet Excitations Mediating Thermally Activated Delayed Fluorescence. *Phys. Rev. Mater.* **2017**, *1*, 075602.
- (39) Zhu, B.; Zhang, L.; Cheng, B.; Yu, J. First-Principle Calculation Study of Tri-s-triazine-Based g-C3N4: A Review. *Appl. Catal. B: Environ.* **2018**, 224, 983–999.
- (40) Liu, A. Y.; Cohen, M. L. Prediction of New Low Compressibility Solids. *Science* 1989, 245, 841–842.
- (41) Corkill, J. L.; Cohen, M. L. Calculated Quasiparticle Band Gap of β -C3N4. *Phys. Rev. B* **1993**, 48, 17622.
- (42) Liu, A. Y.; Wentzcovitch, R. M. Stability of Carbon Nitride Solids. *Phys. Rev. B* **1994**, *50*, 10362.
- (43) Teter, D. M.; Hemley, R. J. Low-Compressibility Carbon Nitrides. *Science* **1996**, 271, 53–55.
- (44) Kroke, E.; Schwarz, M.; Horath-Bordon, E.; Kroll, P.; Noll, B.; Norman, A. D. Tri-s-triazine Derivatives. Part I. From Trichloro-tri-s-triazine to Graphitic C3N4 Structures. *New J. Chem.* **2002**, *26*, 508–512.
- (45) Alves, I.; Demazeau, G.; Tanguy, B.; Weill, F. On a New Model of the Graphitic Form of C3N4. *Solid State Commun.* **1999**, *109*, 697–701.
- (46) Komatsu, T. Prototype Carbon Nitrides Similar to the Symmetric Triangular Form of Melon. J. Mater. Chem. 2001, 11, 802–803
- (47) Xu, Y.; Gao, S.-P. Band Gap of C3N4 in the GW Approximation. Int. J. Hydrogen Energy 2012, 37, 11072-11080.
- (48) Li, H.; Wu, X.; Yin, S.; Katsumata, K.; Wang, Y. Effect of Rutile TiO2 on the Photocatalytic Performance of g-C3N4/Brookite-TiO2-xNy Photocatalyst for NO Decomposition. *Appl. Surf. Sci.* **2017**, 392, 531–539.
- (49) Singh, J. A.; Overbury, S. H.; Dudney, N. J.; Li, M.; Veith, G. M. Gold Nanoparticles Supported on Carbon Nitride: Influence of Surface Hydroxyls on Low Temperature Carbon Monoxide Oxidation. ACS Catal 2012, 2, 1138–1146.
- (50) Lu, C.; Chen, R.; Wu, X.; Fan, M.; Liu, Y.; Le, Z.; Jiang, S.; Song, S. Boron Doped g-C3N4 with Enhanced Photocatalytic UO22+Reduction Performance. *Appl. Surf. Sci.* **2016**, *360*, 1016–1022.
- (51) Lam, S.-M.; Sin, J.-C.; Mohamed, A. R. A Review on Photocatalytic Application of g-C3N4/Semiconductor (CNS) Nanocomposites towards the Erasure of Dyeing Wastewater. *Mater. Sci. Semicon. Proc.* **2016**, *47*, 62–84.
- (52) Aleksandrzak, M.; Kukulka, W.; Mijowska, E. Graphitic Carbon Nitride/Graphene Oxide/Reduced Graphene Oxide Nanocomposites for Photoluminescence and Photocatalysis. *Appl. Surf. Sci.* **2017**, 398, 56–62
- (53) Li, Y.; Xia, Z.; Yang, Q.; Wang, L.; Xing, Y. Review on g-C3N4-Based S-Scheme Heterojunction Photocatalysts. *J. Mater. Sci. Technol.* **2022**, *125*, 128.

- (54) Wang, J.; Wang, S. A Critical Review on Graphitic Carbon Nitride (g-C3N4)-Based Materials: Preparation, Modification and Environmental Application. *Coord. Chem. Rev.* **2022**, 453, 214338.
- (55) Wang, X.; Maeda, K.; Thomas, A.; Takanabe, K.; Xin, G.; Carlsson, J. M.; Domen, K.; Antonietti, M. A Metal-Free Polymeric Photocatalyst for Hydrogen Production from Water under Visible Light. *Nat. Mater.* **2009**, *8*, 76–80.
- (56) Xu, Q.; Jiang, C.; Cheng, B.; Yu, J. Enhanced Visible-Light Photocatalytic H2-Generation Activity of Carbon/g-C3N4 Nanocomposites Prepared by Two-Step Thermal Treatment. *Dalton Trans* **2017**, *46*, 10611–10619.
- (57) Iqbal, W.; Qiu, B.; Lei, J.; Wang, L.; Zhang, J.; Anpo, M. One-Step Large-Scale Highly Active g-C3N4 Nanosheets for Efficient Sunlight-Driven Photocatalytic Hydrogen Production. *Dalton Trans* **2017**, *46*, 10678–10684.
- (58) Li, K.; Su, F.-Y.; Zhang, W.-D. Modification of g-C3N4 Nanosheets by Carbon Quantum Dots for Highly Efficient Photocatalytic Generation of Hydrogen. *Appl. Surf. Sci.* **2016**, 375, 110–117.
- (59) Ling, G. Z. S.; Ng, S.-F.; Ong, W.-J. Tailor-Engineered 2D Cocatalysts: Harnessing Electron—Hole Redox Center of 2D g-C3N4 Photocatalysts toward Solar-to-Chemical Conversion and Environmental Purification. *Adv. Funct. Mater.* **2022**, *32*, 2111875.
- (60) Tan, M.; Ma, Y.; Yu, C.; Luan, Q.; Li, J.; Liu, C.; Dong, W.; Su, Y.; Qiao, L.; Gao, L.; et al. Boosting Photocatalytic Hydrogen Production via Interfacial Engineering on 2D Ultrathin Z-Scheme ZnIn2S4/g-C3N4 Heterojunction. *Adv. Funct. Mater.* **2022**, 32, 2111740.
- (61) Ye, S.; Wang, R.; Wu, M.-Z.; Yuan, Y.-P. A Review on g-C3N4 for Photocatalytic Water Splitting and CO2 Reduction. *Appl. Surf. Sci.* **2015**, 358, 15–27.
- (62) Liu, S.; Chen, F.; Li, S.; Peng, X.; Xiong, Y. Enhanced Photocatalytic Conversion of Greenhouse Gas CO2 into Solar Fuels Over g-C3N4 Nanotubes with Decorated Transparent ZIF-8 Nanoclusters. *Appl. Catal. B: Environ.* **2017**, *211*, 1–10.
- (63) Li, H.; Gao, Y.; Wu, X.; Lee, P.-H.; Shih, K. Fabrication of Heterostructured g-C3N4/Ag-TiO2 Hybrid Photocatalyst with Enhanced Performance in Photocatalytic Conversion of CO2 under Simulated Sunlight Irradiation. *Appl. Surf. Sci.* **2017**, 402, 198–207.
- (64) Sayed, M.; Zhu, B.; Kuang, P.; Liu, X.; Cheng, B.; Ghamdi, A. A. A.; Wageh, S.; Zhang, L.; Yu, J. EPR Investigation on Electron Transfer of 2D/3D g-C3N4/ZnO S-Scheme Heterojunction for Enhanced CO2 Photoreduction. *Adv. Sustain. Syst.* 2022, 6, 2100264.
- (65) Grimme, S. Improved Second-Order Møller—Plesset Perturbation Theory by Separate Scaling of Parallel-and Antiparallel-Spin Pair Correlation Energies. *J. Chem. Phys.* **2003**, *118*, 9095—9102.
- (66) Adamo, C.; Jacquemin, D. The Calculations of Excited-State Properties with Time-Dependent Density Functional Theory. *Chem. Soc. Rev.* **2013**, 42, 845–856.
- (67) Jacquemin, D.; Mennucci, B.; Adamo, C. Excited-State Calculations with TD-DFT: from Benchmarks to Simulations in Complex Environments. *Phys. Chem. Chem. Phys.* **2011**, *13*, 16987–16998.
- (68) Sancho-Garcia, J. C.; Bremond, E.; Ricci, G.; Pérez-Jiménez, A.; Olivier, Y.; Adamo, C. Violation of Hund's Rule in Molecules: Predicting the Excited-State Energy Inversion by TD-DFT with Double-Hybrid Methods. *J. Chem. Phys.* **2022**, *156*, 034105.
- (69) Alipour, M.; Izadkhast, T. Do Any Types of Double-Hybrid Models Render the Correct Order of Excited State Energies in Inverted Singlet—Triplet Emitters? *J. Chem. Phys.* **2022**, *156*, 064302.
- (70) Ghosh, S.; Bhattacharyya, K. Origin of the Failure of Density Functional Theories in Predicting Inverted Singlet—Triplet Gaps. *J. Phys. Chem. A* **2022**, *126*, 1378–1385.
- (71) Dreuw, A.; Head-Gordon, M. Single-Reference ab Initio Methods for the Calculation of Excited States of Large Molecules. *Chem. Rev.* **2005**, *105*, 4009–4037.
- (72) Laurent, A. D.; Jacquemin, D. TD-DFT Benchmarks: A Review. Int. J. Quantum Chem. 2013, 113, 2019–2039.

- (73) Dreuw, A.; Head-Gordon, M. Failure of Time-Dependent Density Functional Theory for Long-Range Charge-Transfer Excited States: the Zincbacteriochlorin- Bacteriochlorin and Bacteriochlorophyll- Spheroidene Complexes. J. Am. Chem. Soc. 2004, 126, 4007—4016.
- (74) Tozer, D. J. Relationship between Long-Range Charge-Transfer Excitation Energy Error and Integer Discontinuity in Kohn-Sham Theory. *J. Chem. Phys.* **2003**, *119*, 12697–12699.
- (75) Gritsenko, O.; Baerends, E. J. Asymptotic Correction of the Exchange—Correlation Kernel of Time-Dependent Density Functional Theory for Long-Range Charge-Transfer Excitations. *J. Chem. Phys.* **2004**, *121*, 655–660.
- (76) Stephens, P. J.; Devlin, F. J.; Chabalowski, C. F.; Frisch, M. J. Ab Initio Calculation of Vibrational Absorption and Circular Dichroism Spectra Using Density Functional Force Fields. *J. Phys. Chem.* **1994**, 98, 11623–11627.
- (77) Iikura, H.; Tsuneda, T.; Yanai, T.; Hirao, K. A Long-Range Correction Scheme for Generalized-Gradient-Approximation Exchange Functionals. *J. Chem. Phys.* **2001**, *115*, 3540–3544.
- (78) Chai, J.-D.; Head-Gordon, M. Systematic Optimization of Long-Range Corrected Hybrid Density Functionals. *J. Chem. Phys.* **2008**, *128*, 084106.
- (79) Grimme, S. Semiempirical Hybrid Density Functional with Perturbative Second-Order Correlation. *J. Chem. Phys.* **2006**, *124*, 034108.
- (80) Karton, A.; Tarnopolsky, A.; Lamère, J.-F.; Schatz, G. C.; Martin, J. M. L. Highly Accurate First-Principles Benchmark Data Sets for the Parametrization and Validation of Density Functional and Other Approximate Methods. Derivation of a Robust, Generally Applicable, Double-Hybrid Functional for Thermochemistry and Thermochemical Kinetics. J. Phys. Chem. A 2008, 112, 12868–12886.
- (81) Casanova-Páez, M.; Dardis, M. B.; Goerigk, L. wB2PLYP and wB2GPPLYP: The First Two Double-Hybrid Density Functionals with Long-Range Correction Optimized for Excitation Energies. *J. Chem. Theory Comput.* **2019**, *15*, 4735–4744.
- (82) Casanova-Páez, M.; Goerigk, L. Assessing the Tamm—Dancoff Approximation, Singlet—Singlet, and Singlet—Triplet Excitations with the Latest Long-Range Corrected Double-Hybrid Density Functionals. *J. Chem. Phys.* **2020**, *153*, 064106.
- (83) Casanova-Páez, M.; Goerigk, L. Time-Dependent Long-Range-Corrected Double-Hybrid Density Functionals with Spin-Component and Spin-Opposite Scaling: A Comprehensive Analysis of Singlet—Singlet and Singlet—Triplet Excitation Energies. *J. Chem. Theory Comput.* **2021**, *17*, 5165—5186.
- (84) Jung, Y.; Lochan, R. C.; Dutoi, A. D.; Head-Gordon, M. Scaled Opposite-Spin Second Order Møller—Plesset Correlation Energy: An Economical Electronic Structure Method. *J. Chem. Phys.* **2004**, *121*, 9793—9802.
- (85) Zhang, Y.; Yang, W. A Challenge for Density Functionals: Self-Interaction Error Increases for Systems with a Noninteger Number of Electrons. *J. Chem. Phys.* **1998**, *109*, 2604–2608.
- (86) Kümmel, S. Charge-Transfer Excitations: A Challenge for Time-Dependent Density Functional Theory That Has Been Met. *Adv. Energy Mater.* **2017**, *7*, 1700440.
- (87) Körzdörfer, T.; Kümmel, S.; Marom, N.; Kronik, L. When to Trust Photoelectron Spectra from Kohn-Sham Eigenvalues: The Case of Organic Semiconductors. *Phys. Rev. B* **2009**, *79*, 201205.
- (88) Tozer, D. J.; Amos, R. D.; Handy, N. C.; Roos, B. O.; Serrano-Andres, L. Does Density Functional Theory Contribute to the Understanding of Excited States of Unsaturated Organic Compounds? *Mol. Phys.* **1999**, *97*, 859–868.
- (89) Maitra, N. T. Double and Charge-Transfer Excitations in Time-Dependent Density Functional Theory. *Annu. Rev. Phys. Chem.* **2022**, 73, 117–140.
- (90) Huix-Rotllant, M.; Ipatov, A.; Rubio, A.; Casida, M. E. Assessment of Dressed Time-Dependent Density-Functional Theory for the Low-Lying Valence States of 28 Organic Chromophores. *Chem. Phys.* **2011**, 391, 120–129.

- (91) Grimme, S.; Neese, F. Double-Hybrid Density Functional Theory for Excited Electronic States of Molecules. *J. Chem. Phys.* **2007**, *127*, 154116.
- (92) Head-Gordon, M.; Rico, R. J.; Oumi, M.; Lee, T. J. A Doubles Correction to Electronic Excited States from Configuration Interaction in the Space of Single Substitutions. *Chem. Phys. Lett.* **1994**, 219, 21–29.
- (93) Schwabe, T.; Goerigk, L. Time-Dependent Double-Hybrid Density Functionals with Spin-Component and Spin-Opposite Scaling. *J. Chem. Theory Comput.* **2017**, *13*, 4307–4323.
- (94) Goerigk, L.; Moellmann, J.; Grimme, S. Computation of Accurate Excitation Energies for Large Organic Molecules with Double-Hybrid Density Functionals. *Phys. Chem. Chem. Phys.* **2009**, *11*, 4611–4620.
- (95) Rhee, Y. M.; Head-Gordon, M. Scaled Second-Order Perturbation Corrections to Configuration Interaction Singles: Efficient and Reliable Excitation Energy Methods. *J. Phys. Chem. A* **2007**, *111*, 5314–5326.
- (96) Goerigk, L.; Grimme, S. A Thorough Benchmark of Density Functional Methods for General Main Group Thermochemistry, Kinetics, and Noncovalent Interactions. *Phys. Chem. Chem. Phys.* **2011**, *13*, 6670–6688.
- (97) Mehta, N.; Casanova-Páez, M.; Goerigk, L. Semi-Empirical or Non-Empirical Double-Hybrid Density Functionals: Which Are More Robust? *Phys. Chem. Chem. Phys.* **2018**, *20*, 23175–23194.
- (98) Dreuw, A.; Hoffmann, M. The Inverted Singlet-Triplet Gap: A Vanishing Myth? Front. Chem. 2023, 11, 1239604.
- (99) Ricci, G.; San-Fabián, E.; Olivier, Y.; Sancho-García, J.-C. Singlet-Triplet Excited-State Inversion in Heptazine and Related Molecules: Assessment of TD-DFT and ab Initio Methods. *ChemPhysChem* **2021**, 22, 553–560.
- (100) Aizawa, N.; Pu, Y.-J.; Harabuchi, Y.; Nihonyanagi, A.; Ibuka, R.; Inuzuka, H.; Dhara, B.; Koyama, Y.; Nakayama, K.-i.; Maeda, S.; et al. Delayed Fluorescence from Inverted Singlet and Triplet Excited States. *Nature* **2022**, *609*, 502–506.
- (101) Li, J.; Li, Z.; Liu, H.; Gong, H.; Zhang, J.; Yao, Y.; Guo, Q. Organic Molecules with Inverted Singlet-Triplet Gaps. Front. Chem. 2022, 10, 999856.
- (102) Drwal, D.; Matousek, M.; Golub, P.; Tucholska, A.; Hapka, M.; Brabec, J.; Veis, L.; Pernal, K. The Role of Spin Polarization and Dynamic Correlation in Singlet-Triplet Gap Inversion of Heptazine Derivatives. arXiv preprint arXiv:2307.09075, 2023,
- (103) Schirmer, J. Beyond the Random-Phase Approximation: A New Approximation Scheme for the Polarization Propagator. *Phys. Rev. A* **1982**, *26*, 2395.
- (104) Christiansen, O.; Koch, H.; Jørgensen, P. The Second-Order Approximate Coupled Cluster Singles and Doubles Model CC2. *Chem. Phys. Lett.* **1995**, 243, 409–418.
- (105) Stanton, J. F.; Bartlett, R. J. The Equation of Motion Coupled-Cluster Method. A Systematic Biorthogonal Approach to Molecular Excitation Energies, Transition Probabilities, and Excited State Properties. J. Chem. Phys. 1993, 98, 7029–7039.
- (106) Andersson, K.; Malmqvist, P. Å.; Roos, B. O. Second-Order Perturbation Theory with a Complete Active Space Self-Consistent Field Reference Function. *J. Chem. Phys.* **1992**, *96*, 1218–1226.
- (107) Leupin, W.; Wirz, J. Low-Lying Electronically Excited States of Cycl[3.3.3] Azine, A Bridged 12.pi.-Perimeter. *J. Am. Chem. Soc.* **1980**, *102*, 6068–6075.
- (108) Ceder, O.; Vernmark, K. Synthesis of the 1,3,4-Triaza- and 1,4-Diazacycl [3.3.3] Azine Systems. *Acta Chem. Scand.* **1977**, 31b, 235–238.
- (109) Leupin, W.; Magde, D.; Persy, G.; Wirz, J. 1,4,7-Triazacycl [3.3.3] Azine: Basicity, Photoelectron Spectrum, Photophysical Properties. *I. Am. Chem. Soc.* **1986**, *108*, 17–22.
- (110) Ceder, O.; Andersson, J. E.; Sæthre, L. J.; Näslund, M.; Svensson, S. The Synthesis of 1,3,6-Triazacycl [3.3.3] Azines. *Acta Chem. Scand.* 1972, 26, 596–610.

- (111) Rossman, M. A.; Leonard, N. J.; Urano, S.; LeBreton, P. R. Synthesis and Valence Orbital Structures of Azacycl [3.3.3] Azines in a Systematic Series. *J. Am. Chem. Soc.* **1985**, *107*, 3884–3890.
- (112) Shahbaz, M.; Urano, S.; LeBreton, P. R.; Rossman, M. A.; Hosmane, R. S.; Leonard, N. J. Tri-s-triazine: Synthesis, Chemical Behavior, and Spectroscopic and Theoretical Probes of Valence Orbital Structure. *J. Am. Chem. Soc.* 1984, 106, 2805–2811.
- (113) Zheng, H.; Chen, W.; Gao, H.; Wang, Y.; Guo, H.; Guo, S.; Tang, Z.; Zhang, J. Melem: An Efficient Metal-Free Luminescent Material. *J. Mater. Chem. C* **2017**, *5*, 10746–10753.
- (114) Ricci, G.; Sancho-García, J.-C.; Olivier, Y. Establishing Design Strategies for Emissive Materials with an Inverted Singlet—Triplet Energy Gap (INVEST): A Computational Perspective on How Symmetry Rules the Interplay between Triplet Harvesting and Light Emission. J. Mater. Chem. C 2022, 10, 12680—12698.
- (115) Sobolewski, A. L.; Domcke, W. Are Heptazine-Based Organic Light-Emitting Diode Chromophores Thermally Activated Delayed Fluorescence or Inverted Singlet—Triplet systems? *J. Phys. Chem. Lett.* **2021**, *12*, 6852–6860.
- (116) Li, J.; Li, Z.; Liu, H.; Gong, H.; Zhang, J.; Li, X.; Wang, Y.; Guo, Q. Down-Conversion-Induced Delayed Fluorescence via an Inverted Singlet-Triplet Channel. *Dyes Pigm* **2022**, 203, 110366.
- (117) Neese, F. The ORCA Program System. WIREs Comput. Mol. Sci. 2012, 2, 73–78.
- (118) Neese, F.; Wennmohs, F.; Becker, U.; Riplinger, C. The ORCA Quantum Chemistry Program Package. *J. Chem. Phys.* **2020**, 152, 224108.
- (119) Weigend, F.; Ahlrichs, R. Balanced Basis Sets of Split Valence, Triple Zeta Valence and Quadruple Zeta Valence Quality for H to Rn: Design and Assessment of Accuracy. *Phys. Chem. Chem. Phys.* **2005**, *7*, 3297–3305.
- (120) Lin, Y.-S.; Li, G.-D.; Mao, S.-P.; Chai, J.-D. Long-Range Corrected Hybrid Density Functionals with Improved Dispersion Corrections. *J. Chem. Theory Comput.* **2013**, *9*, 263–272.
- (121) Grimme, S.; Antony, J.; Ehrlich, S.; Krieg, H. A Consistent and Accurate ab Initio Parametrization of Density Functional Dispersion Correction (DFT-D) for the 94 Elements H-Pu. *J. Chem. Phys.* **2010**, 132, 154104.
- (122) Neese, F. Software Update: The ORCA Program System—Version 5.0. Wiley Interdiscip. Rev.: Comput. Mol. Sci. 2022, 12, No. e1606.
- (123) Hellweg, A.; Hättig, C.; Höfener, S.; Klopper, W. Optimized Accurate Auxiliary Basis Sets for RI-MP2 and RI-CC2 Calculations for the Atoms Rb to Rn. *Theor. Chem. Acc.* **2007**, *117*, 587–597.